LANGMUIR

pubs.acs.org/Langmuir Article

# Magnetically Controllable Isotropic/Anisotropic Slippery Surface for Flexible Droplet Manipulation

Yao Fang, Jie Liang, Xue Bai, Jiale Yong, Jinglan Huo, Qing Yang,* Xun Hou, and Feng Chen*

Cite This: *Langmuir* 2020, 36, 15403−15409 Read Online

ACCESS | Metrics & More | Article Recommendations | Supporting Information

**ABSTRACT:** Controllable wetting surfaces play a significant role in numerous applications such as smart liquid manipulation, lab-on-a-chip, drug delivery, liquid robot, and so on. A novel type of magnetically controllable isotropic/anisotropic slippery surface was prepared by femtosecond laser ablation. The slippery liquid-infused porous surface (SLIPS) can be switched between an isotropic smooth state and an anisotropic groove state by the magnetic field. The relationship between the sliding property of the SLIPS and the magnetic flux density, water droplet volume, microgroove width, and microgroove height are systematically studied. Passively flexible movement on the isotropic SLIPS and actively directional movement on the anisotropic SLIPS of water droplets were realized. This work provides a fresh understanding of the controllable isotropic/anisotropic SLIPS and reveals great potential in versatile applications which are related to magnetically controllable smart liquid manipulation.

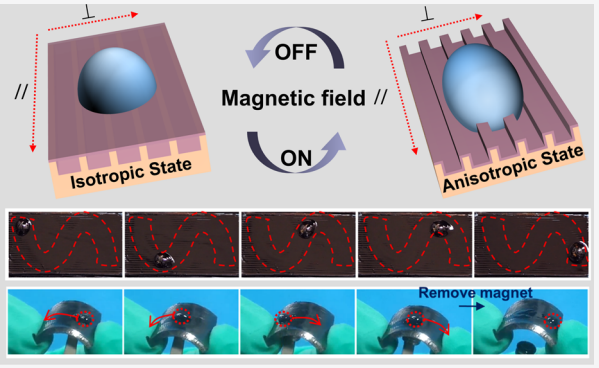




## INTRODUCTION

*The Nepenthes*-inspired slippery liquid-infused porous surface (SLIPS) has attracted extensive attention in the past decade because of the great range of applications, such as anti-icing coating, antifouling surface, material protection, biomedical devices, and so on.[1−7] Compared to the lotus leaf-inspired superhydrophobic surface, SLIPS has remarkable repellence to a wider range of objects including various kinds of liquids with different surface tensions, composite solution with different components, biological liquids such as blood or tissue fluid, and even cells or insects.[8−12]

All SLIPSs include a porous substrate and a smooth lubricant layer. Usually, a special porous substrate with an anisotropic microstructure can endow the SLIPS with anisotropic properties.[13−15] Limited by the fabrication methods of the porous substrate, obviously, there are more studies about the isotropic SLIPS than the anisotropic SLIPS.[8,15−21] In practical applications, an anisotropic SLIPS is as important as an isotropic SLIPS because of the more outstanding controllability to different kinds of liquids. In addition, introducing external stimulus-responsive properties into a SLIPS can immeasurably enhance the flexibility and intelligence of the SLIPS in different applications.[22−30] Benefited from elastic substrates, the tunable isotropic and anisotropic SLIPS was realized by direction mechanical stretching.[31,32] Luo at al. prepared the tunable isotropic/anisotropic SLIPS on the shape-memory polymer by the replica-molding process.[33] Through the groove template-pressing process and heating recovery process, the SLIPS was switched between an isotropic SLIPS and an anisotropic SLIPS. However, these tunable isotropic/anisotropic SLIPSs are all relied on the restorable substrate. It restricts the realization of the tunable isotropic/anisotropic SLIPS on other materials which are not elastic or do not have shape-memory properties. This extremely limits the application of the tunable isotropic/anisotropic SLIPS. Thus, a new strategy for realizing the tunable isotropic/anisotropic SLIPS which does not rely on the changing of the substrate is still challenging and desperately in need. It can enable more flexible liquid manipulation and dramatically expand the application fields of the SLIPS.

Herein, a kind of magnetically controllable isotropic/anisotropic SLIPS was prepared by femtosecond laser ablation. A directionally porous microgroove array was constructed directly by two-step femtosecond laser ablation. After chemical modification and ferrofluid infusion, the magnetically responsive SLIPS was prepared. Through the magnetic field-controlled ferrofluid transfer and the ferrofluid self-backflow process, the SLIPS can be switched between the isotropic state and the anisotropic state. At the anisotropic state, the

**Received:** October 15, 2020
**Revised:** November 27, 2020
**Published:** December 8, 2020





https://dx.doi.org/10.1021/acs.langmuir.0c03008
*Langmuir* 2020, 36, 15403−15409

anisotropic sliding property can be tuned by different magnetic flux densities. The wettability of the extremely anisotropic-state SLIPS is strongly related to the water droplet volume, microgroove width ($L$), and microgroove height, while the isotropic-state SLIPS is hardly affected by these. At the isotropic state, flexible liquid movement was realized on both horizontal and tilted flat SLIPSs and even the curved SLIPS surface. At the anisotropic state, directional water droplet transportation and in situ water droplet coalescing were achieved. Magnetically controllable on−off control of the circuit was achieved by the movement and location of a conductive liquid droplet on the SLIPS. This study will improve the understanding of design and preparation of isotropic and anisotropic SLIPSs. The prepared magnetically controllable isotropic/anisotropic SLIPS can be applied in smart droplet manipulation, lab-on-a-chip, drug delivery, liquid robot, and so on.

## EXPERIMENTAL SECTION

**Materials.** Diglycidyl ether of bisphenol A (DGEBA) was obtained from Nantong Xingchen Synthetic Material Co., Ltd. *n*-Octylamine (OA) was purchased from J&K Scientific Ltd. *m*-Xylylenediamine (MXDA) was obtained from J&K Scientific Ltd. The ferrofluid MF02 was purchased from Beijing Shenjan Ferrofluid Technological Co., Ltd. More information of the ferrofluid MF02 is given in Figure S1. All reagents were directly used without any further treatment. OA, MXDA, and DGEBA are mixed in a molar ratio of 1:2:5. A subsequent bubble removing process was carried out in a vacuum oven for about 20 min with a temperature of 30 °C. After that, the mixture was cured at 60 °C for 2 h and 100 °C for 1 h. So far, the substrate of the SLIPS, a kind of epoxy polymer (EP), was synthesized.

**Fabrication of the SLIPS.** The femtosecond laser is produced by a regenerative amplified Ti:sapphire laser system (Coherent Libra-USP-HE). The center wavelength is 800 nm. The frequency is 1 kHz, while the pulse width is 50 fs. The substrate was fixed on a precision stage in advance. The femtosecond laser beam was focused on the substrate surface by an objective lens (5×, NA = 0.15). A predetermined computer program was used to control the movement of the stage to control the laser ablation process. The whole fabrication process of the SLIPS includes four steps, as shown in Figure 1a. First, the whole substrate surface was ablated by the femtosecond laser (laser power = 20 mW) with a typical line-by-line scanning process. The scanning speed was set at 8 mm/s, while the line interval was 8 $\mu$m. Second, the microgroove array was built on the laser-ablated substrate by selective femtosecond laser ablation. The microgroove width ($L$) was set ranging from 500 to 800 $\mu$m. The interval of each microgroove was set at 60 $\mu$m all the time. The microgroove height can be tuned by adjusting the laser power. Third, the sample with the microgroove array was cleaned with deionized water in an ultrasonic washer for about 10 min. After drying naturally, the sample was immersed in 0.5 vol % fluoroalkylsilane (FAS, 1*H*,1*H*,2*H*,2*H*-perfluorodecyltrimethoxysilane, Aladdin) ethanol solution for 12 h. A subsequent curing process of the self-assembly FAS layer was carried out in an oven at 40 °C for 4 h. Finally, the ferrofluid was dripped on the sample. The magnetic field was used to assist to infuse the ferrofluid into the porous microgroove array.

**Characterization.** The magnetic field was produced by a cylindrical neodymium magnet whose diameter and height are both 10 mm. The magnetic flux density was measured using an HT20 teslameter (Shanghai Hengtong Magnetoelectric Technological Co., Ltd, China). The contacting angle (CA) and sliding angle (SA) were tested using a JC2000D CA system (Powereach, China). Each average value was obtained from five test values. Scanning electron microscopy (SEM) photographs were obtained using a Flex 1000 scanning electron microscope (Hitachi, Japan). A LEXT-OLS4000 laser confocal microscope (Olympus, Japan) was used to get the three-dimensional topography and the corresponding profile curves.

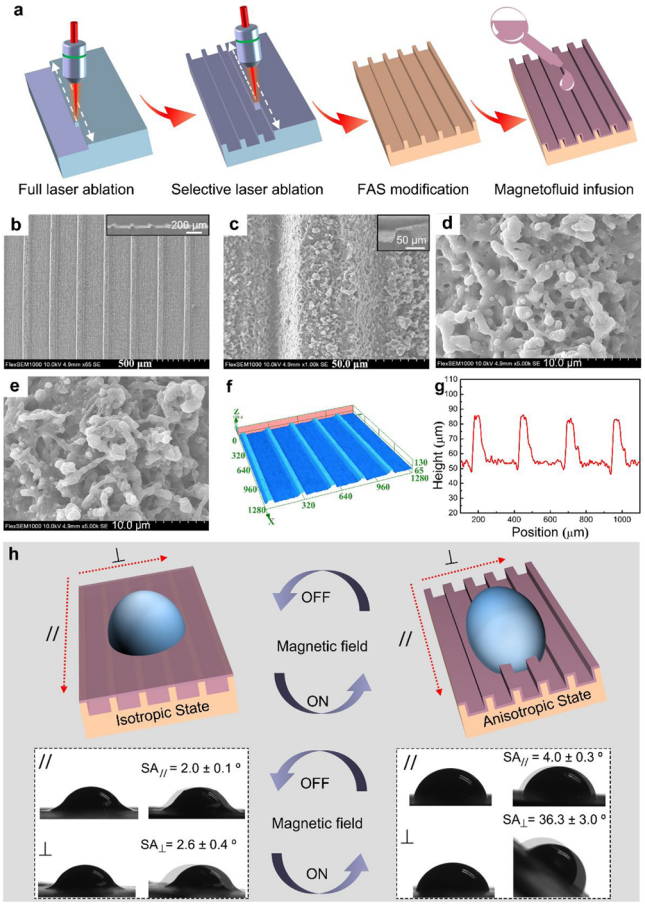


**Figure 1.** (a) Schematic diagram of the preparation process of the controllable isotropic/anisotropic SLIPS. (b−g) Morphology of the laser-ablated porous microgroove structure ($L$ = 200 $\mu$m and height = 27.5 ± 0.8 $\mu$m). (h) Controllable isotropic/anisotropic SLIPS by controlling the magnetic field. Water droplet sliding in parallel and perpendicular directions on both the smooth-state SLIPS and the groove-state SLIPS.

The height of the slippery groove array was also measured by the LEXT-OLS4000.

## RESULTS AND DISCUSSION

The porous structure is indispensable to prepare the SLIPS. The periodically directional microscale structure can induce anisotropic wettability. As shown in Figure S2a, the peristome of *Nepenthes* is covered by a kind of microgroove structure with the width of several hundreds of micrometers and the height of several tens of micrometers. The *Nepenthes* peristome is naturally wet and slippery. Because of the anisotropic slippery peristome, insects tend to slip along the microgroove into the pitcher. After wetting by water, the water was transported to the outside of the peristome and evaporated. The water layer decreased during the transportation and evaporation process, as shown in Figure S2b, which induced different heights of the wetting microgroove array. Imitating the tunable height of the wetting microgroove may be effective to achieve tunable anisotropic slippery properties without changing the substrate.

After two steps of femtosecond laser ablation, the porously directional microgroove array was built on the EP surface, as shown in Figure 1b−e. The ridges between each microgroove have steep side walls. Both the bottom surface of the microgrooves (Figure 1d) and the top surface of the ridges


https://dx.doi.org/10.1021/acs.langmuir.0c03008
Langmuir 2020, 36, 15403−15409

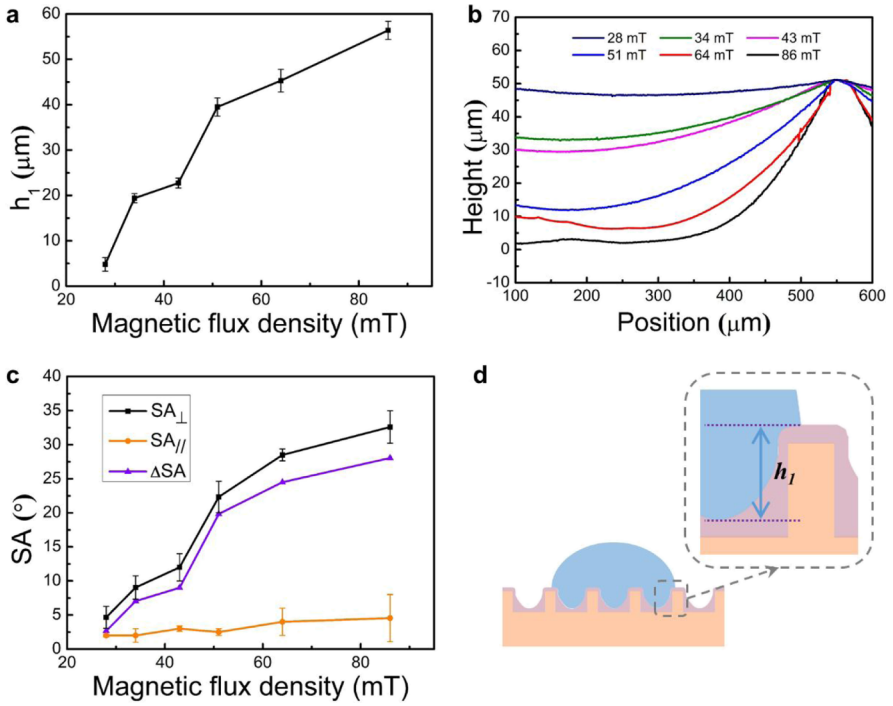


**Figure 2.** (a) Relationship between the height of the slippery groove and the magnetic flux density. (b) Profile image of the SLIPS under different magnetic flux densities. (c) Tunable SA of a water droplet (3 $\mu$L) on the SLIPS in the parallel and perpendicular directions under different magnetic flux densities. (d) Schematic cross-sectional diagram of a water droplet on the groove-state SLIPS in the perpendicular direction.

(Figure 1e) are covered with sufficient rough structures. Lots of holes with the size ranging from a few hundreds of nanometers to several micrometers were also constructed on the ablated surface, simultaneously. Whether from the SEM images (Figure 1b,c) or the 3D confocal microscopy image (Figure 1f) or the corresponding profile image, the width and height of microgrooves are uniform. The height of each microgroove shows a linear relationship with the femtosecond laser power, as shown in Figure S3. When the laser power was set at 40 mW during the second laser ablation step, the built microgroove showed a height of 27.5 ± 0.8 $\mu$m.

The wettability of a water droplet and a ferrofluid droplet on the FAS-modified porous microgroove array ($L$ = 700 $\mu$m and height = 61.3 ± 1.9 $\mu$m) is shown in Figure S4. After infusing the ferrofluid, the magnetically controllable SLIPS was prepared, as shown in Figure 1h. The SA in the parallel direction of microgrooves is defined as $SA_{\parallel}$, while the SA in perpendicular direction is defined as $SA_{\perp}$. Before applying the magnetic field (defined as the smooth state), the SLIPS shows isotropic slippery properties. SAs show a negligible difference in the parallel and perpendicular directions. On the smooth-state SLIPS, the $SA_{\parallel}$ of a 3 $\mu$L water droplet is 2.0 ± 0.1°, while the $SA_{\perp}$ is 2.6 ± 0.4°. Interestingly, because of the magnetic field (≥86 mT)-induced transfer of the ferrofluid in the microgrooves, the microgroove structure appears (defined as the groove state) and shows anisotropic slippery properties. The transferred ferrofluid was locked by the magnetic field at the edge of the sample. On the groove-state SLIPS, a water droplet (3 $\mu$L) shows a much bigger $SA_{\perp}$ of 36.3 ± 3.0° than an $SA_{\parallel}$ of 4.0 ± 0.3°. Because a part of the water droplet is inserted into the slippery microgrooves, it results in a bigger resistance in the perpendicular direction. After removing the magnetic field, the ferrofluid can flow back to the original microgrooves, which induces the anisotropic SLIPS to recover the isotropic SLIPS. Thus, a kind of controllable isotropic/anisotropic SLIPS is realized by controlling the magnetic field without changing the substrate.

The anisotropic sliding property of the SLIPS (substrate $L$ = 700 $\mu$m and height = 61.3 ± 1.9 $\mu$m) can be tuned by different magnetic flux densities. The magnetic flux density can be changed by adjusting the distance above the magnet top surface, as shown in Figure S5. The height of slippery microgrooves increases with increasing magnetic flux density, as shown in Figure 2a. When the magnetic flux density is 28 mT, the SLIPS barely shows a groove structure which only has a height of 4.8 ± 1.5 $\mu$m. The SLIPS shows almost the original groove structure with a height of 56.4 ± 2.0 $\mu$m after applying a magnetic flux density of 86 mT. A bigger magnetic flux density can induce more ferrofluid to be transferred, which caused a higher height of the slippery microgrooves. Figure 2b shows the profile image of the SLIPS under different magnetic flux densities. More importantly, the SLIPS can be changed from almost isotropic to anisotropic by controlling the magnetic flux density, as shown in Figure 2c. The difference value between $SA_{\perp}$ and $SA_{\parallel}$ increases from 2.7 to 28.1° with increasing magnetic flux density. Interestingly, the changing trend of the $SA_{\perp}$ (Figure 2c) is very similar to that of the height of the slippery microgrooves (Figure 2a), which indicates the linear relationship between the $SA_{\perp}$ and the height. As shown in Figure 2d, the height of the inserted parts of a water droplet ($h_1$) is determined by the height of slippery microgrooves. A bigger inserted height causes a bigger resistance to the water droplet, which produces a bigger SA along the perpendicular direction. Thus, a kind of magnetically tunable anisotropic SLIPS is realized by adjusting the height of the slippery microgroove.

The limit value of the tunable range of the SA on the SLIPS is closely related to the water droplet volume, substrate


https://dx.doi.org/10.1021/acs.langmuir.0c03008
Langmuir 2020, 36, 15403−15409

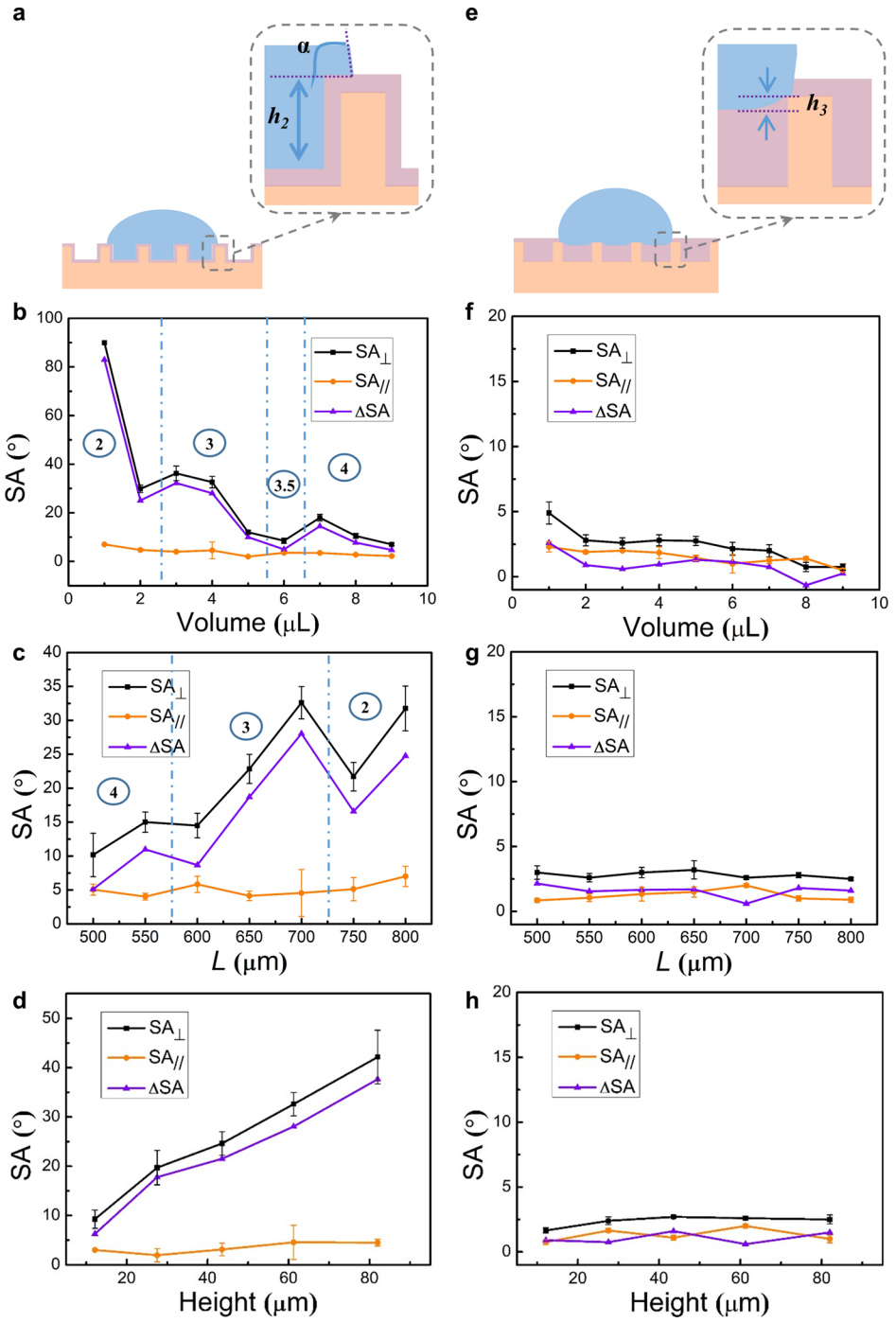


**Figure 3.** (a) Schematic cross-sectional diagram of a water droplet on the groove-state SLIPS in the perpendicular direction. (b–d) Relationship between the SA value and water droplet volume (b), groove width $L$ (c), and groove height (d) on the groove-state SLIPS, when the magnetic field is no less than 86 mT. (e) Schematic cross-sectional diagram of a water droplet on the smooth-state SLIPS in the perpendicular direction. (f–h) Relationship between the SA value and water droplet volume (f), groove width $L$ (g), and groove height (h) on the smooth-state SLIPS, when the magnetic field is no more than 28 mT.

microgroove width, and height. Figure 3a–d shows the anisotropic property of the extreme groove-state SLIPS (magnetic field ≥ 86 mT), while Figure 3e–h shows the isotropic property of the smooth-state SLIPS (magnetic field ≤ 28 mT). For different water droplet volume tests, the width and height of the SLIPS substrate microgrooves are 700 and 61.3 ± 1.9 $\mu$m, respectively. Figure 3b is divided into four parts according to the number ($N$) of the microgrooves that the water droplet inserts. As shown in Figure S6, when the water droplet volume is no more than 2 $\mu$L, the $N$ is 2, which increases to 3 (3–5 $\mu$L) and 3.5 (6 $\mu$L) and then to 4 (7–9 $\mu$L). When the $N$ is the same, the $SA_{\perp}$ decreases with increasing water droplet volume, which is caused by increasing CA (Figure S6) and increasing gravity. A bigger CA means a smaller sliding resistance, while the increasing gravity means a bigger diving force. At the critical value (2–3 and 5–7 $\mu$L), the CA decreases with increasing water droplet volume (Figure S6). Thus, there is a slight increase in $SA_{\perp}$ when the volume


https://dx.doi.org/10.1021/acs.langmuir.0c03008
Langmuir 2020, 36, 15403–15409

increases at the critical value. For different $N$ values, an obvious decrease in $SA_{\perp}$ is caused by the multiplied water droplet gravity. In the parallel direction, $SA_{\parallel}$ is always smaller than 5° except 1 $\mu$L ($SA_{\parallel} = 7 \pm 0.2°$).

As shown in Figure 3c,d, the $SA_{\perp}$ of the extreme groove-state SLIPS is closely related to the morphological features of the substrate microgroove array. The volume of the water droplet used in the test, in Figure 3c,d, is 3 $\mu$L. As shown in Figure 3c, when the $L$ increases from 500 to 800 $\mu$m, the $SA_{\perp}$ shows a fluctuation rule, while the $SA_{\parallel}$ shows little change. The water droplet inserts into four microgrooves ($N = 4$) when the $L$ ranges from 500 to 550 $\mu$m, while the $N$ changes to three ($L = 600-700$ $\mu$m) and two ($L = 750-800$ $\mu$m). When the $N$ is the same, the $SA_{\perp}$ increases with increasing $L$. A larger $L$ means that a larger proportion of the water droplet inserts into these microgrooves, which induces a smaller CA. Thus, a bigger resistance effect of microgrooves is generated with increasing $L$, which causes an increasing $SA_{\perp}$. At the critical value (550−600 and 700−750 $\mu$m), there is an obvious decline of $SA_{\perp}$ because of decreasing $N$ and CA. In the parallel direction, the microgroove width $L$ shows a negligible effect on the $SA_{\parallel}$.

The $SA_{\perp}$ shows a quasi-linear relationship with the microgroove height. A higher height of microgrooves induces a higher height of the inserted water droplet parts ($h_2$, Figure 3a). Thus, a bigger resistance is produced when a water droplet slides in the perpendicular direction. However, in the parallel direction, there is no influence of the $h_2$ to the $SA_{\parallel}$. Thus, the difference between $SA_{\perp}$ and $SA_{\parallel}$ increases with increasing height of the slippery microgrooves. On the isotropic smooth-state SLIPS, water droplets can only insert a negligible height ($h_3$) into the microgrooves, as shown in Figure 3e. Therefore, only a slight difference between $SA_{\perp}$ and $SA_{\parallel}$ is produced, as shown in Figure 3f−h. The sliding property on the isotropic smooth-state SLIPS is almost unrelated to the water droplet volume, microgroove width, and microgroove height.

Passively flexible movement of water droplets can be easily realized on the isotropic smooth-state SLIPS by controlling the magnetic field. As shown in Figure S7a, a water droplet slipped down freely on the tilted (10°) isotropic smooth-state SLIPS. When the magnetic field was applied at the target place in the slipping path of the water droplet, the slipping water droplet stopped at that place immediately. Once the magnetic field was turned off, the water droplet recovered the slippery state, as shown in Figure S7b. The water droplet even slipped upward on the tilted SLIPS, which was controlled by the movement of the magnetic field (Figure 4a-1). Flexible movement of a water droplet on the flat isotropic smooth SLIPS was realized by controlling the movement of the magnetic field, as shown in Figure 4a-2 ("S") and Figure S7c ("Z", "C"). Benefiting from the shape-memory property of the substrate, the SLIPS can be changed to different shapes. As shown in Figure 4a-3, the SLIPS was curved and a flexible movement of a water droplet was achieved on the curved SLIPS. The magnetically controllable movement of a water droplet was benefited from the isotropic slippery property and ferrofluid coating layer.

Actively directional water droplet movement was achieved on the anisotropic groove-state SLIPS. As shown in Figure 4b-1, a glass slide was tilted at 10° ($\theta_1$) in advance. The anisotropic SLIPS was fixed on it along the direction that the angle ($\theta_2$) between the groove direction and the direction of the gravity component along the slope was 15°. Driven by the gravity, the water droplet slipped along the groove direction

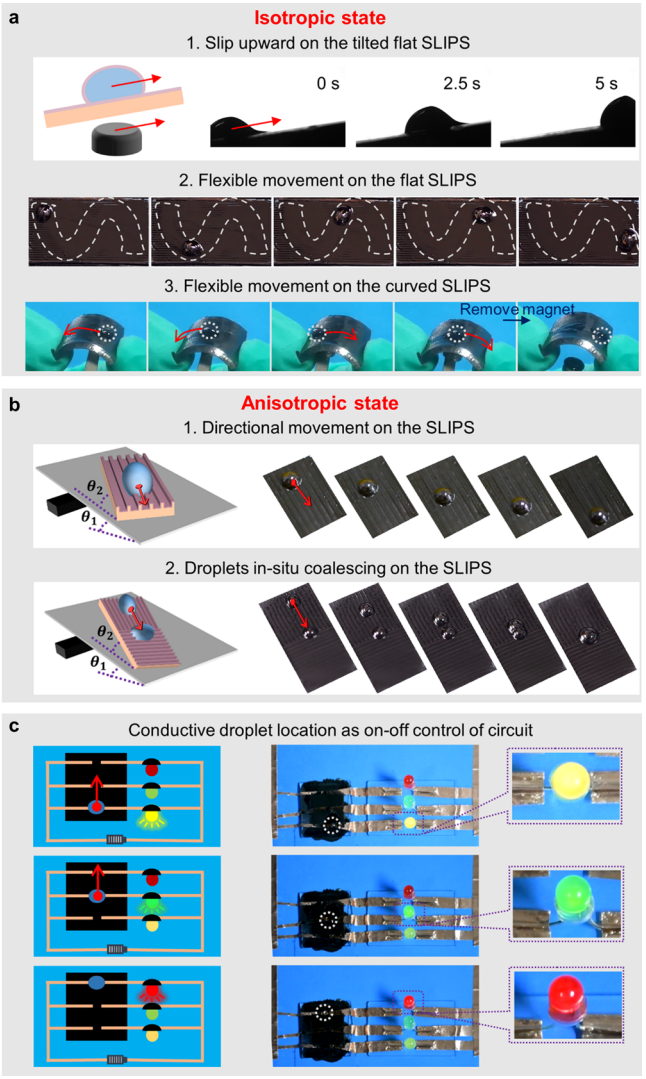


**Figure 4.** (a) Passively flexible movement of water droplets on the smooth-state SLIPS: (1) slipping upward on the tilted SLIPS and (2,3) flexible movement on the flat (2) and curved (3) SLIPS. (b) Actively directional water droplet movement: (1) directional sliding and (2) droplet in situ coalescing. (c) On−off control of the circuit by manipulating a conductive liquid droplet to locate at different positions on the SLIPS surface.

rather than the direction of the gravity component because of the anisotropic property of the SLIPS. On this basis, water droplet in situ coalescing was realized. The $\theta_1$ is smaller than $SA_{\perp}$ but larger than $SA_{\parallel}$. Thus, the water droplet directionally slid to contact and coalesced with the pinned water droplet, as shown in Figure 4b-2.

Using a conductive droplet (saturated NaCl solution), a magnetically controlled liquid on−off control of the electrical circuit was achieved on the SLIPS. As shown in Figure 4c, a simple parallel circuit was designed. Each branch circuit was broken at the original state. When the conductive droplet was moved and located at the broken position of each branch circuit, the yellow, green, and red lights were lighted in order. More potential applications can be developed because of the magnetically controllable movement of the liquid droplet.


https://dx.doi.org/10.1021/acs.langmuir.0c03008
Langmuir 2020, 36, 15403−15409

## CONCLUSIONS

A kind of magnetically controllable isotropic/anisotropic slippery surface was prepared by femtosecond laser ablation. The SLIPS can be switched between the anisotropic groove state and isotropic smooth state by magnetic field without changing the substrate. The anisotropic property can be tuned by magnetic flux density, water droplet volume, microgroove width, and microgroove height. Passively flexible movement of the water droplet on tilted, flat, and curved isotropic SLIPSs was controlled by the movement of the magnetic field. Actively directional water droplet movement and droplet in situ coalescing were achieved on the anisotropic SLIPS. On−off control of the electrical circuit was carried out by controlling the movement and location of a conductive droplet on the SLIPS. The magnetically controllable isotropic/anisotropic SLIPS will give a fresh understanding of isotropic and anisotropic SLIPSs and can be applied in smart droplet manipulation, drug delivery, liquid robot, lab-on-a-chip, and other related fields.

## ASSOCIATED CONTENT

### Supporting Information

The Supporting Information is available free of charge at https://pubs.acs.org/doi/10.1021/acs.langmuir.0c03008.

Parameters of the ferrofluid MF02; optical image and SEM image of *Nepenthes*; linear relationship between microgroove height and femtosecond laser power; wettability of the FAS-modified porous microgroove array; relationship between magnetic flux density and the distance; water droplets of different volumes on the anisotropic groove-state SLIPS; and water droplets' movement on the isotropic smooth-state SLIPS (PDF)

Controllable movement of water droplets on the SLIPS (Movie S1) (MP4)

## AUTHOR INFORMATION


### Corresponding Authors

**Qing Yang** − *School of Mechanical Engineering, Xi'an Jiaotong University, Xi'an 710049, PR China*; Email: yangqing@mail.xjtu.edu.cn

**Feng Chen** − *State Key Laboratory for Manufacturing System Engineering and Shaanxi Key Laboratory of Photonics Technology for Information, School of Electronic Science and Engineering, Xi'an Jiaotong University, Xi'an 710049, PR China*; orcid.org/0000-0002-7031-7404; Email: chenfeng@mail.xjtu.edu.cn

### Authors

**Yao Fang** − *State Key Laboratory for Manufacturing System Engineering and Shaanxi Key Laboratory of Photonics Technology for Information, School of Electronic Science and Engineering, Xi'an Jiaotong University, Xi'an 710049, PR China*

**Jie Liang** − *State Key Laboratory for Manufacturing System Engineering and Shaanxi Key Laboratory of Photonics Technology for Information, School of Electronic Science and Engineering, Xi'an Jiaotong University, Xi'an 710049, PR China*

**Xue Bai** − *State Key Laboratory for Manufacturing System Engineering and Shaanxi Key Laboratory of Photonics Technology for Information, School of Electronic Science and Engineering, Xi'an Jiaotong University, Xi'an 710049, PR China*

**Jiale Yong** − *State Key Laboratory for Manufacturing System Engineering and Shaanxi Key Laboratory of Photonics Technology for Information, School of Electronic Science and Engineering, Xi'an Jiaotong University, Xi'an 710049, PR China*

**Jinglan Huo** − *State Key Laboratory for Manufacturing System Engineering and Shaanxi Key Laboratory of Photonics Technology for Information, School of Electronic Science and Engineering, Xi'an Jiaotong University, Xi'an 710049, PR China*

**Xun Hou** − *State Key Laboratory for Manufacturing System Engineering and Shaanxi Key Laboratory of Photonics Technology for Information, School of Electronic Science and Engineering, Xi'an Jiaotong University, Xi'an 710049, PR China*

Complete contact information is available at: https://pubs.acs.org/10.1021/acs.langmuir.0c03008


### Notes

The authors declare no competing financial interest.

## ACKNOWLEDGMENTS

This work is supported by the National Science Foundation of China under the grant no. 61875158, the National Key Research and Development Program of China under the grant no. 2017YFB1104700, the International Joint Research Laboratory for Micro/Nano Manufacturing and Measurement Technologies, and the Fundamental Research Funds for the Central Universities.

## REFERENCES


(1) Kim, P.; Wong, T.-S.; Alvarenga, J.; Kreder, M. J.; Adorno-Martinez, W. E.; Aizenberg, J. Liquid-infused nanostructured surfaces with extreme anti-ice and anti-frost performance. *ACS Nano* **2012**, *6*, 6569−6577.

(2) Amini, S.; Kolle, S.; Petrone, L.; Ahanotu, O.; Sunny, S.; Sutanto, C. N.; Hoon, S.; Cohen, L.; Weaver, J. C.; Aizenberg, J.; Vogel, N.; Miserez, A. Preventing mussel adhesion using lubricant-infused materials. *Science* **2017**, *357*, 668−673.

(3) Wang, P.; Lu, Z.; Zhang, D. Slippery liquid-infused porous surfaces fabricated on aluminum as a barrier to corrosion induced by sulfate reducing bacteria. *Corros. Sci.* **2015**, *93*, 159−166.

(4) Liu, Y.-Q.; Jiao, Z.-Z.; Zhang, Y.-L.; Liu, Y.; Jiang, H.-B.; Han, D.-D.; Sun, H.-B. Kraft Mesh Origami for Efficient Oil-Water Separation. *Langmuir* **2019**, *35*, 815−823.

(5) Wu, Q.; Yang, C.; Su, C.; Zhong, L.; Zhou, L.; Hang, T.; Lin, H.; Chen, W.; Li, L.; Xie, X. Slippery Liquid-Attached Surface for Robust Biofouling Resistance. *ACS Biomater. Sci. Eng.* **2020**, *6*, 358−366.

(6) Long, Y.; Yin, X.; Mu, P.; Wang, Q.; Hu, J.; Li, J. Slippery liquid-infused porous surface (SLIPS) with superior liquid repellency, anti-corrosion, anti-icing and intensified durability for protecting substrates. *Chem. Eng. J.* **2020**, *401*, 126137.

(7) Xie, Y.; Li, J.; Bu, D.; Xie, X.; He, X.; Wang, L.; Zhou, Z. Nepenthes-inspired multifunctional nanoblades with mechanical bactericidal, self-cleaning and insect anti-adhesive characteristics. *RSC Adv.* **2019**, *9*, 27904−27910.

(8) Li, J.; Ueda, E.; Paulssen, D.; Levkin, P. A. Slippery Lubricant-Infused Surfaces: Properties and Emerging Applications. *Adv. Funct. Mater.* **2019**, *29*, 1802317.

(9) Yong, J.; Huo, J.; Yang, Q.; Chen, F.; Fang, Y.; Wu, X.; Liu, L.; Lu, X.; Zhang, J.; Hou, X. Femtosecond Laser Direct Writing of Porous Network Microstructures for Fabricating Super-Slippery

Surfaces with Excellent Liquid Repellence and Anti-Cell Proliferation. *Adv. Mater. Interfaces* **2018**, *5*, 1701479.
(10) Fang, Y.; Yong, J.; Chen, F.; Huo, J.; Yang, Q.; Zhang, J.; Hou, X. Bioinspired Fabrication of Bi/Tridirectionally Anisotropic Sliding Superhydrophobic PDMS Surfaces by Femtosecond Laser. *Adv. Mater. Interfaces* **2018**, *5*, 1701245.
(11) Gorb, E. V.; Gorb, S. N. The effect of surface anisotropy in the slippery zone of Nepenthes alata pitchers on beetle attachment. *Beilstein J. Nanotechnol.* **2011**, *2*, 302−310.
(12) Sunny, S.; Cheng, G.; Daniel, D.; Lo, P.; Ochoa, S.; Howell, C.; Vogel, N.; Majid, A.; Aizenberg, J. Transparent antifouling material for improved operative field visibility in endoscopy. *Proc. Natl. Acad. Sci. U.S.A.* **2016**, *113*, 11676−11681.
(13) Lv, X.; Jiao, Y.; Wu, S.; Li, C.; Zhang, Y.; Li, J.; Hu, Y.; Wu, D. Anisotropic Sliding of Underwater Bubbles On Microgrooved Slippery Surfaces by One-Step Femtosecond Laser Scanning. *ACS Appl. Mater. Interfaces* **2019**, *11*, 20574−20580.
(14) Wang, B. L.; Heng, L.; Jiang, L. Temperature-Responsive Anisotropic Slippery Surface for Smart Control of the Droplet Motion. *ACS Appl. Mater. Interfaces* **2018**, *10*, 7442−7450.
(15) Guo, T.; Che, P.; Heng, L.; Fan, L.; Jiang, L. Anisotropic Slippery Surfaces: Electric-Driven Smart Control of a Drop's Slide. *Adv. Mater.* **2016**, *28*, 6999−7007.
(16) Manna, U.; Raman, N.; Welsh, M. A.; Zayas-Gonzalez, Y. M.; Blackwell, H. E.; Palecek, S. P.; Lynn, D. M. Slippery Liquid-Infused Porous Surfaces that Prevent Microbial Surface Fouling and Kill Non-Adherent Pathogens in Surrounding Media: A Controlled Release Approach. *Adv. Funct. Mater.* **2016**, *26*, 3599−3611.
(17) Deng, R.; Shen, T.; Chen, H.; Lu, J.; Yang, H.-C.; Li, W. Slippery liquid-infused porous surfaces (SLIPSs): a perfect solution to both marine fouling and corrosion? *J. Mater. Chem. A* **2020**, *8*, 7536−7547.
(18) Wang, Z.; Heng, L.; Jiang, L. Effect of lubricant viscosity on the self-healing properties and electrically driven sliding of droplets on anisotropic slippery surfaces. *J. Mater. Chem. A* **2018**, *6*, 3414−3421.
(19) Li, H.; Feng, X.; Peng, Y.; Zeng, R. Durable lubricant-infused coating on a magnesium alloy substrate with anti-biofouling and anti-corrosion properties and excellent thermally assisted healing ability. *Nanoscale* **2020**, *12*, 7700−7711.
(20) Che, P.; Heng, L.; Jiang, L. Lubricant-Infused Anisotropic Porous Surface Design of Reduced Graphene Oxide Toward Electrically Driven Smart Control of Conductive Droplets' Motion. *Adv. Funct. Mater.* **2017**, *27*, 1606199.
(21) Wang, Z.; Liu, Y.; Guo, P.; Heng, L.; Jiang, L. Porous Films: Photoelectric Synergetic Responsive Slippery Surfaces Based on Tailored Anisotropic Films Generated by Interfacial Directional Freezing. *Adv. Funct. Mater.* **2018**, *28*, 1870350.
(22) Irajizad, P.; Hasnain, M.; Farokhnia, N.; Sajadi, S. M.; Ghasemi, H. Magnetic slippery extreme icephobic surfaces. *Nat. Commun.* **2016**, *7*, 13395.
(23) Wu, S.; Zhou, L.; Chen, C.; Shi, L.-A.; Zhu, S.; Zhang, C.; Meng, D.; Huang, Z.; Li, J.; Hu, Y.; Wu, D. Photothermal Actuation of Diverse Liquids on an Fe3O4-Doped Slippery Surface for Electric Switching and Cell Culture. *Langmuir* **2019**, *35*, 13915−13922.
(24) Wang, Y.; Qian, B.; Lai, C.; Wang, X.; Ma, K.; Guo, Y.; Zhu, X.; Fei, B.; Xin, J. H. Flexible Slippery Surface to Manipulate Droplet Coalescence and Sliding, and Its Practicability in Wind-Resistant Water Collection. *ACS Appl. Mater. Interfaces* **2017**, *9*, 24428−24432.
(25) Wang, J.; Sun, L.; Zou, M.; Gao, W.; Liu, C.; Shang, L.; Gu, Z.; Zhao, Y. Bioinspired shape-memory graphene film with tunable wettability. *Sci. Adv.* **2017**, *3*, No. e1700004.
(26) Liu, C.; Ding, H.; Wu, Z.; Gao, B.; Fu, F.; Shang, L.; Gu, Z.; Zhao, Y. Tunable Structural Color Surfaces with Visually Self-Reporting Wettability. *Adv. Funct. Mater.* **2016**, *26*, 7937−7942.
(27) Wang, J.; Gao, W.; Zhang, H.; Zou, M.; Chen, Y.; Zhao, Y. Programmable wettability on photocontrolled graphene film. *Sci. Adv.* **2018**, *4*, No. eaat7392.
(28) Manabe, K.; Matsubayashi, T.; Tenjimbayashi, M.; Moriya, T.; Tsuge, Y.; Kyung, K.-H.; Shiratori, S. Controllable Broadband Optical Transparency and Wettability Switching of Temperature-Activated Solid/Liquid-Infused Nanofibrous Membranes. *ACS Nano* **2016**, *10*, 9387−9396.
(29) Gao, C.; Wang, L.; Lin, Y.; Li, J.; Liu, Y.; Li, X.; Feng, S.; Zheng, Y. Droplets Manipulated on Photothermal Organogel Surfaces. *Adv. Funct. Mater.* **2018**, *28*, 1803072.
(30) Cao, M.; Jin, X.; Peng, Y.; Yu, C.; Li, K.; Liu, K.; Jiang, L. Unidirectional Wetting Properties on Multi-Bioinspired Magneto-controllable Slippery Microcilia. *Adv. Mater.* **2017**, *29*, 1606869.
(31) Roy, P. K.; Pant, R.; Nagarajan, A. K.; Khare, K. Mechanically Tunable Slippery Behavior on Soft Poly(dimethylsiloxane)-Based Anisotropic Wrinkles Infused with Lubricating Fluid. *Langmuir* **2016**, *32*, 5738−5743.
(32) Zhang, Y.; Jiao, Y.; Chen, C.; Zhu, S.; Li, C.; Li, J.; Hu, Y.; Wu, D.; Chu, J. Reversible Tuning between Isotropic and Anisotropic Sliding by One-Direction Mechanical Stretching on Microgrooved Slippery Surfaces. *Langmuir* **2019**, *35*, 10625−10630.
(33) Luo, X.; Lai, H.; Cheng, Z.; Liu, P.; Li, Y.; Yu, X.; Liu, Y. Slippery shape memory polymer arrays with switchable isotropy/anisotropy and its application as a reprogrammable platform for controllable droplet motion. *Chem. Eng. J.* **2021**, *403*, 126356.


https://dx.doi.org/10.1021/acs.langmuir.0c03008
*Langmuir* 2020, 36, 15403−15409